SINGLE-CRYSTAL TIME-OF-FLIGHT NEUTRON DIFFRACTION

Arthur J. Schultz

IPNS Division, Argonne National Laboratory

Argonne, IL 60439 USA

ABSTRACT

The single-crystal time-of-flight (TOF) Laue technique combines the use of a large-area position-sensitive detector (PSD) with a range of incident neutron wavelengths available from a pulsed neutron source. With a stationary sample and detector, a three-dimensional sampling of reciprocal space is obtained that may contain hundreds of Bragg reflections. In addition, all of reciprocal space between the peaks is also measured simultaneously making this technique highly advantageous for studying pressure and temperature dependent phase transitions. Instruments designed for this purpose are also uniquely useful in texture studies of polycrystalline samples. The technique and instruments in use at IPNS (Argonne), LANSCE (Los Alamos) and ISIS (Rutherford) will be described. Examples of studies ranging from the modulated structure of an organic superconductor to the magnetic form factor of a high-T_C related compound are presented .

INTRODUCTION

The single-crystal time-of-flight (TOF) Laue technique can be traced back nearly forty years to a 1956 paper by R. D. Lowde[1] in which it is proposed that:

> The Laue method of recording integrated intensities, with certain adjuncts, appears to be in many ways simpler than the rotating-crystal method. A proposed technique is discussed, which is particularly suitable for use with pulsed neutron sources such as

> electron accelerators....The apparatus required, however, has more to go wrong, and it will require some effort to establish the technique in the first place.

In the intervening years much effort has gone into establishing the technique and using it for scientific purposes. This paper will attempt to describe the results of those efforts.

A brief historical survey is presented in Table 1. Currently, there are single-crystal TOF Laue instruments with area PSDs at the IPNS (Argonne, USA),[2] LANSCE (Los Alamos, USA),[3] ISIS (RAL, UK),[4] and the KENS (KEK, Japan)[5] pulsed spallation neutron sources. For obvious reasons of familiarity, most of the discussion in this paper will involve experiments at the IPNS. Other papers in this volume highlight results obtained at LANSCE[6] and ISIS.[7]

Description of the TOF Laue Technique

At the IPNS, the source is pulsed at 30 Hz, such that neutrons emerge from the moderators every $33\frac{1}{3}$ msec. The neutrons sort themselves by velocity v, which is related to wavelength λ by the de Broglie equation $\lambda = \frac{h}{mv} = (\frac{h}{m})(\frac{t}{L})$, where h is Planck's constant, m is the neutron mass,

TABLE 1

Brief history of the development of the single-crystal time-of-flight Laue technique

1956	Lowde[1] proposes time-of-flight Laue method for use with pulsed sources such as electron accelerators.
1965	Buras *et al.*[8] experimentaly demonstrate single crystal TOF Laue technique using chopped beams from steady state reactor sources.
1970	Day and Sinclair[9] obtain single-crystal data using the Harwell electron linac and a curved array of scintillation detectors.
1979	Balagurov *et al.*[10] collect and analyze single crystal data at a pulsed reactor source.
1980	Niimura *et al.*[11] measure diffuse scattering using a 1-D detector at an electron linac source.
1981	Peterson and coworkers[12,13] describe the collection and analysis of single crystal data using an area PSD at a pulsed spallation neutron source (ZING-P').

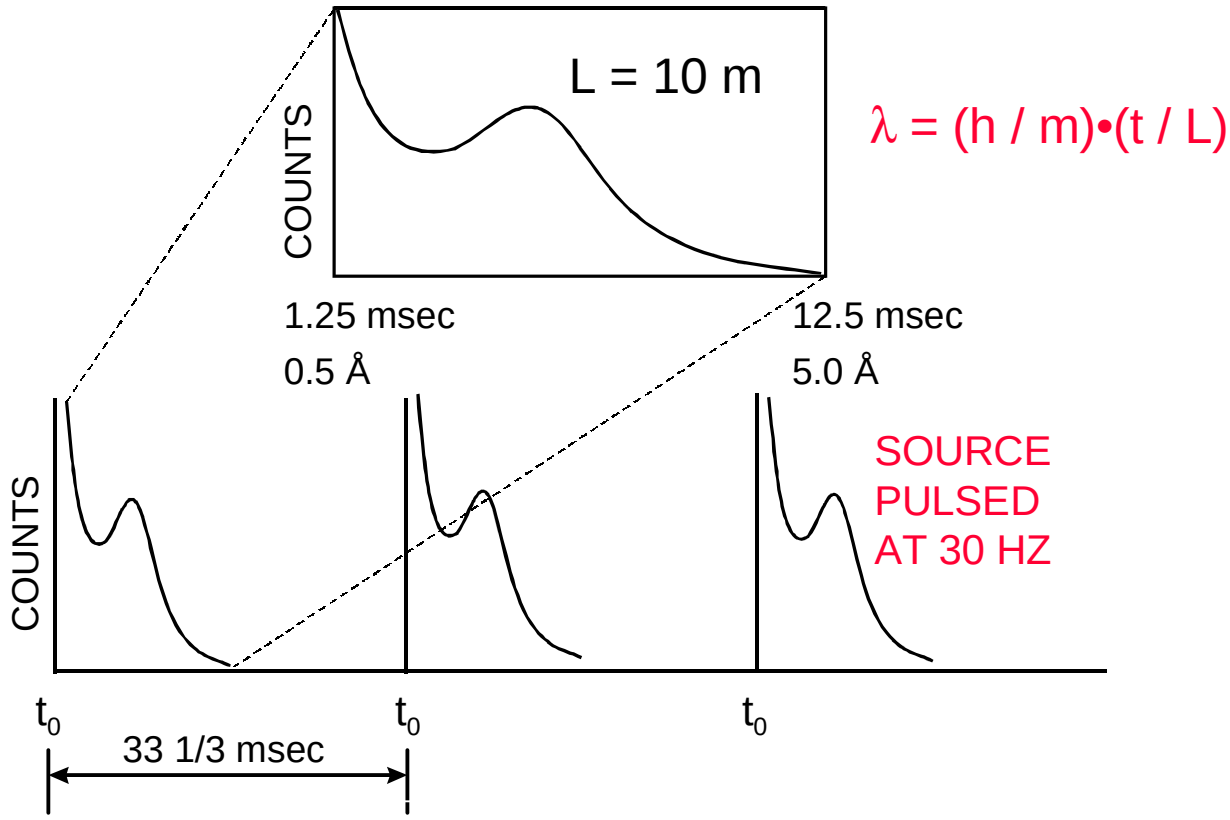

Figure 1. Incident spectrum vs. TOF and wavelength.

and t is the TOF for pathlength L. A possible spectrum for a flight path of 10 m is shown in Figure 1. In a conventional diffraction experiment at a steady state source, the duty cycle is 100% but only a small portion ($< 10^{-2}$) of the available neutrons are selected using a monochromator with typical reflectivity of 50% or less. At a pulsed source utilizing the TOF Laue technique in the example in Figure 1, the duty cycle is reduced to 33%, but there is no monochromator (therefore no second order contamination) and all of the thermal, in addition to some epithermal, neutrons are used.

Figure 2 depicts the Ewald spheres for the minimum wavelength (λ_{min} at t_{min}) and the maximum wavelength (λ_{max} at t_{max}) during each pulse of neutrons. With a stationary crystal and with a stationary *point* detector at $2\theta = 90°$, four Bragg reflections along a *linear* reciprocal lattice vector can be measured "simultaneously" since they will satisfy the Bragg condition $\lambda_n =$

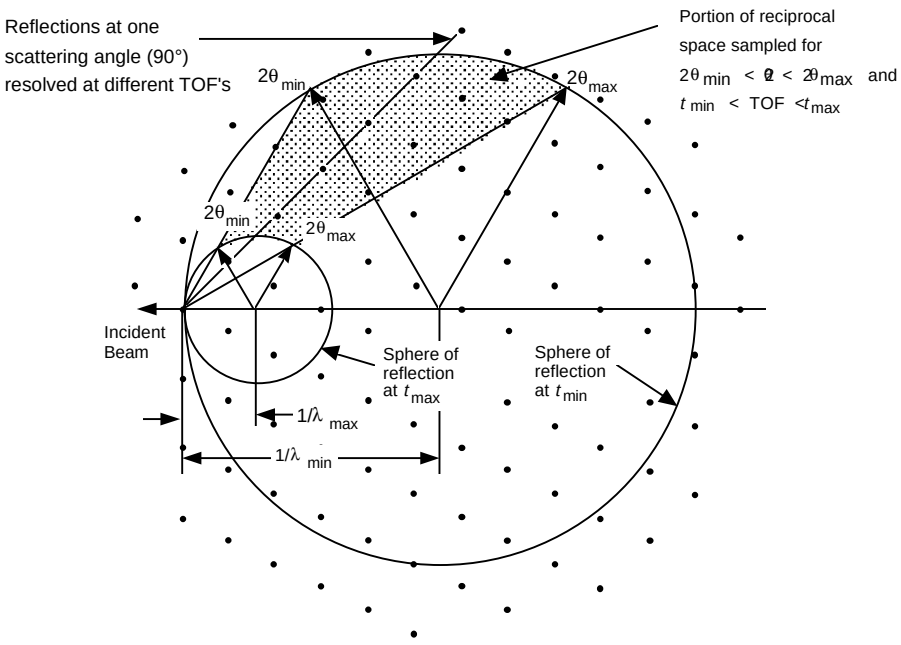

Figure 2. Spheres of reflection in reciprocal space for the minimum and maximum wavelengths at the minium and maximum TOF's.

$2d_n\sin\theta$ at different times-of-flight, where *n* in Figure 2 varies from 2 to 5. With a *linear* position-sensitive detector (PSD) spanning the range from $2\theta_{min}$ to $2\theta_{max}$, all of the Bragg peaks within the shaded *area* could be measured. Going one step further, a two-dimensional *area* PSD will sample a solid *volume* of reciprocal space which may contain hundreds of Bragg peaks. This feature of the TOF Laue technique with a large area PSD is particularly useful in the measurement of numerous high Q data. This was the case in the studies of magnetostriction in MnF_2,[14] and more recently in FeF_2 and NiF_2,[15,16] for which λ_{min} of 0.4 Å was used, yielding data with $Q_{max} = 4\pi(\sin\theta)/\lambda_{min}$ Å 25 $Å^{-1}$, and with d_{min} Å 0.25 Å.

Another important feature of the technique is that not just the Bragg peaks are measured, but all of reciprocal space within a solid volume is sampled. This is advantageous for searching and measuring satellite and superlattice reflections and diffuse scattering. Structural and magnetic phase transitions associated with varying temperature or pressure can be observed and characterized without an *a priori* knowledge of where in reciprocal space the new scattering will appear, as for example in the study of the phase transitions in proustite (Ag_3AsS_3)[17] and in

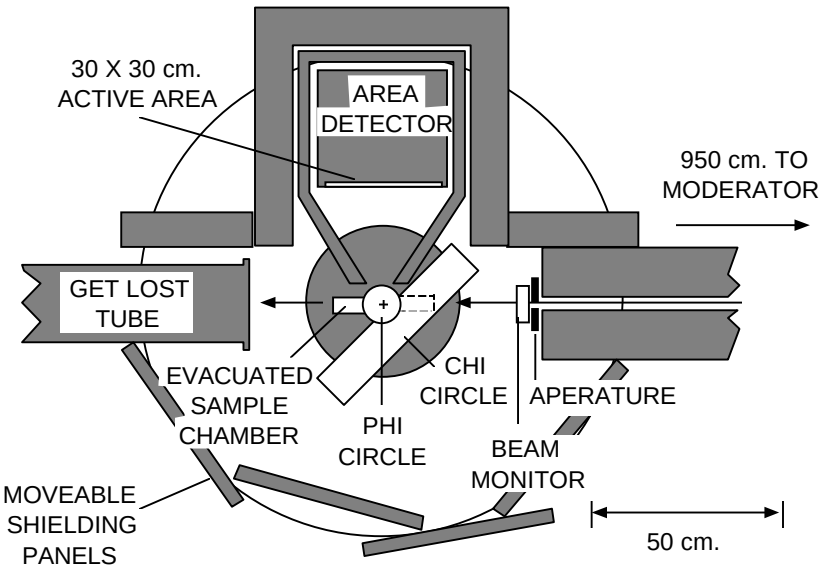

Figure 3. Top view of the IPNS SCD. Fixed parameters are $\omega = 45°$, detector angle = 90°, and sample-to-detector disastance = 32 cm.

organic[18] and copper oxide[19] superconductors described below. Diffuse scattering measurements at ISIS are described in this volume by D. A. Keen.[7] Another feature which has been exploited at LANSCE and IPNS is the use of the single crystal instruments for texture and preferred orientation analyses of polycrystalline samples, as described in this volume by H.-R. Wenk.[6,20]

A schematic representation of the IPNS single crystal diffractometer (SCD) is shown in Figure 3. The crystal orienter consists of Huber χ and ϕ circles with full 360° rotation about ϕ and rotation about χ from the 90° (lower left in Figure 3) to the 180° (top of χ circle) positions. The ω angle (45°), the detector angle (90°), the sample-to-detector distance (32 cm), and the sample-to-moderator distance (950 cm), are fixed. This configuration requires ~35 settings of χ and ϕ to cover a full hemisphere of reciprocal space. The area PSD is a ^{6}Li-glass scintillation detector with a positional resolution of ~3 mm.[21] Each detected neutron is characterized by three histogram coordinates x,y,t representing horizontal and vertical detector positions and time-of-flight, respectively. The time channel widths Δt are varied such that the time (wavelength) resolution $\Delta t/t$ is constant for all TOFs (wavelengths). The histogram coordinates can be mapped

into *hkl* reciprocal lattice coordinates and plotted in various ways when searching for superlattice and satellite reflections.

The sample orienter for the LANSCE SCD[3] has a fixed χ angle of 60°. The area PSD is positioned above the horizontal plane permitting nearly 360° rotations of the ϕ and ω angles so that full spherical coverage is approached. The ^{3}He gas-filled multiwire detector has an active area of 25 x 25 cm^2.

The ISIS SXD has a ^{6}Li-containing ZnS scintillation PSD with optical fiber encoding and an active are of 20 x 20 cm^2. It is described in an accompanying paper in this volume.[7]

The first step of a typical data collection is to mount a crystal on the instrument and begin accumulating a histogram of data. At the IPNS, the active histogram data are displayed on a terminal screen and Bragg peaks can often become visible within minutes. A search program will locate and store the positions of peaks in a reflection file and an autoindexing program[22] is then used to obtain a unit cell and the crystal orientation. Thus, spending hours centering the crystal and finding and centering peaks with a conventional instrument at a steady state source is avoided. This also means that the design and operation of environmental equipment (temperature, pressure) is easier since alignment requirements are less stringent and, during actual data collection, the sample is stationary. Based on the symmetry and orientation of the crystal, the χ and ϕ angles of 10 to 35 histograms are selected in order to cover a unique region of reciprocal space. Each histogram is typically measured for 2 to 8 hours, depending on the crystal quality and volume, the unit cell volume, and the available beam time. Bragg intensities are obtained by calculating peak positions in each histogram and integrating in three dimensions by fitting a box around the peak[23] or by use of an ellipsoidal contour technique which maximizes the $I/\sigma(I)$ ratio[24].

The integrated intensities I_{hkl} are reduced to structure factor amplitudes $|F_{hkl}|$ based on the Laue formula:[8,25]

$$I_{hkl} = k\, \tau(\lambda)\, \phi(\lambda)\, \varepsilon(\lambda,\boldsymbol{r})\, A(\lambda)\, y(\lambda)\, |F_{hkl}|^2\, \lambda^4 / \sin^2\Theta$$

where k is a scale factor and $\tau(\lambda)$ is the deadtime loss. The incident flux spectrum $\phi(\lambda)$ is obtained by measuring the incoherent scattering from a vanadium sample. The detector efficiency $\varepsilon(\lambda,\boldsymbol{r})$ is calculated as a function of wavelength λ and position $\boldsymbol{r}$ on the detector for each Bragg peak since the slant path through the flat ^{6}Li glass varies with $\boldsymbol{r}$. Sample absorption $A(\lambda)$ includes the wavelength dependence of the linear absroption coefficients. Because of the large wavelength dependence of extinction, equivalent data are not averaged and the extinction correction $y(\lambda)$ is evaluated during the least-squares refinement of the structure.

The set of structure factor amplitudes which are obtained at this point can be used to refine a structure using conventional least-squares methods. In an accompanying paper in this volume, the accuracy of IPNS SCD results are shown to be good in a comparison with monochromatic neutron and γ-ray results from the same crystals.[16]

Each of the single crystal instruments have low temperature capabilities with a closed cycle helium refrigerator and in some cases, with liquid helium. A sample pressure of 20 kbar at room temperature was achieved in a study of Tl_3PSe_4 at LANSCE.[3] At the IPNS, a pressure of 5 kbar is achievable while simultaneously cooling the sample on a Displex cold stage. High temperature experiments at the IPNS include a study of yttria-stabilized zirconia, $Zr(Y)O_{1.862}$, at 767°C,[26] and of the nonlinear optical material thallium titanyl phosphate, $TlTiOPO_4$, at 650°C, well above its ferroelectric-to-paraelectric phase transition (T_c = 583°C).[27]

Some additional selected examples of scientific results obtained with the IPNS SCD are described below.

SCIENTIFIC ACHIEVEMENTS

A C–H···Metal Interaction

The activation of a C–H bond by a metal is a critical step in many catalytic reactions. High precision neutron diffraction structural results are necessary to characterize the arrangement of the three atoms and the degree of electron delocalization in stable molecules containing 3-center C–H···metal bonds. The first full crystal and molecular structure analysis on a TOF Laue instrument was that of methylcyclohexenylmanganese tricarbonyl, $Mn(CO)_3(C_7H_{11})$.[28] As shown in Figure 4, the most important feature of the structure is the C(1)–H(1A)–Mn interaction with H(1A) located almost exactly in an octahedral site about the manganese atom and with a very long C(1)–H(1A) distance of 1.19(1) Å. This compares to an average value of 1.09(1) Å for the

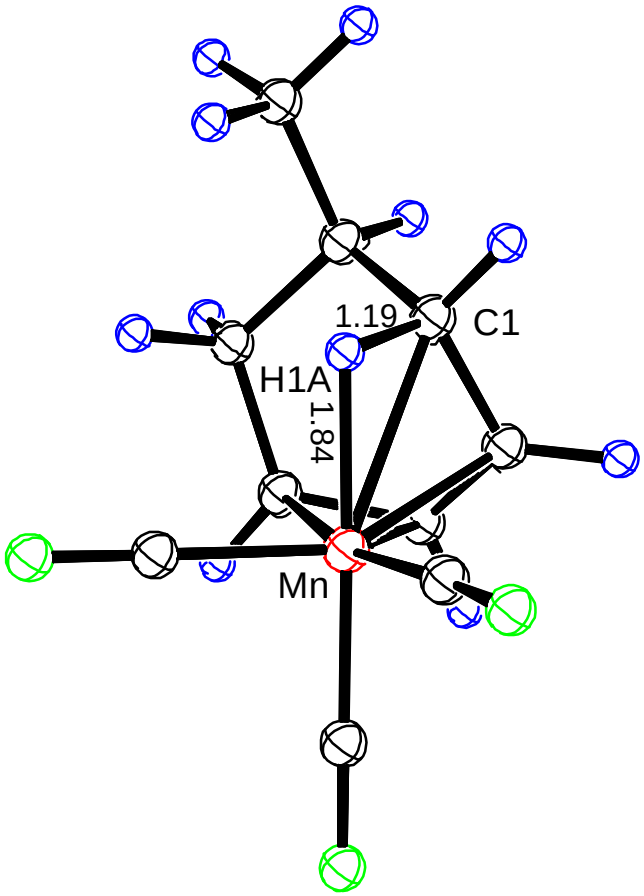

Figure 4. Molecular structure of $Mn(CO)_3(C_7H_{11})$ showing the strong C–H–Mn interaction.

other C–H distances in the structure, as expected. The relatively large esd values are due to the limited data set resulting from instrumental problems associated with this first experiment. If the C–H···metal bond is ignored, the molecule formally contains 16 valence electrons. An 18-electron configuration is achieved only by delocalization of the two electrons in the C(1)–H(1A) bond to form a 3-center, 2-electron C(1)–H(1A)–Mn bond.

Organics Superconductors

Organic superconductors have been the subject of a number of investigations on the SCD. The first of these involved the characterizations of the low temperature commensurate superlattices in the quasi-one-dimensional charge transfer salts $(TMTSF)_2X$, where $X^- = ClO_4^-$ or BF_4^-, both of which have T_c's of 1–2 K.[29] The superlattices are due to ordering of the tetrahedral anions which are located on centers of inversion in the high temperature structural phases.

The largest number of organic superconductors and those with the highest T_c values known to date are based on the donor molecule BEDT-TTF, or simply ET.[30] Whereas the TMTSF salts are all nearly isostructural, ET salts crystallize with many different structural phases, even with the same anion and stoichiometry. Most of the salts are layered materials with layers of conducting donor molecules sandwiched between layers of anions.

One of the most interesting features of the ET molecule is the occurrence of different conformations as depicted in Figure 5, and the relation of these conformations to lattice softness, disorder, and T_c. In the case of β-$(ET)_2I_3$, we have characterized three distinct structural phases. At room temperature and ambient pressure, each ET molecule assumes a random orientation with either an eclipsed or staggered conformation of their ethylene groups. In 1984, the observation of incommensurate superlattice satellite reflections with x-rays and with neutrons on the SCD from crystals of β-$(ET)_2I_3$ below ~200 K was reported.[18] These satellite reflections were shown to be due to displacive modulations of the I_3^- anions and the ET molecules as rigid groups and to

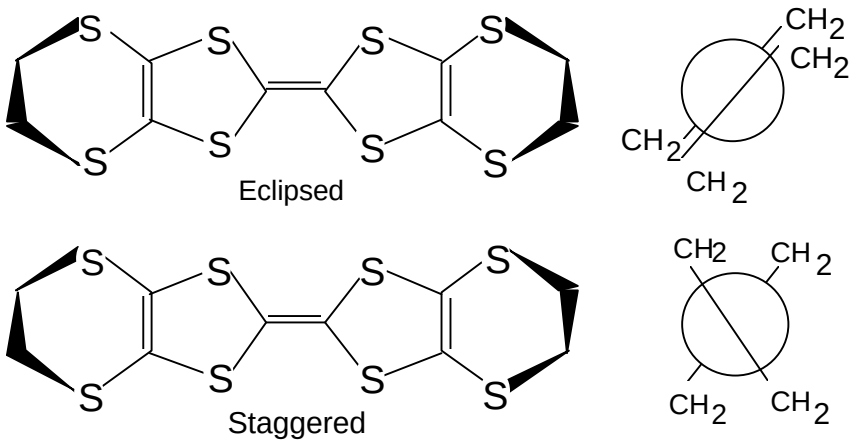

Figure 5. The two ethylene group arrangements of ET. The C–S and C–C bonds of the ethylenedithio units (S–CH_2–CH_2–S) are represented by wedges to distinguish the C atoms lying above and below the molecular π-framework. The diagrams on the right depict the eclipsed and staggered arrangements of the ethylene groups when viewed parallel to the central C=C double bond.

modulation of the above-mentioned conformational disorder.[31] Upon further cooling, β-$(ET)_2I_3$ becomes superconducting at T_c = 1.4 K, which compares to T_c = 2.8 K for β-$(ET)_2IBr_2$ and T_c = 4.98 K for β-$(ET)_2AuI_2$ with ET molecules in ordered eclipsed conformations. The low T_c for β-$(ET)_2I_3$ was attributed to its partial disorder (incommensurate modulation) although it was predicted to have the highest T_c based on band calculations of the density of states at the Fermi energy.

Then, in 1985 it was reported that T_c for β-$(ET)_2I_3$ rises from ~1 K at ambient pressure to ~8 K with applied pressures above 1.2-1.3 kbar.[32,33] A helium high pressure sample cell which mounts on the Displex cold stage of the SCD was designed and fabricated to investigate the high pressure phase. Using this equipment, it was observed that the satellite reflections, which are present at ambient pressure below 200 K, are absent above a critical pressure of 0.5 kbar applied at room temperature and followed by cooling, as shown in Figure 6.[34] The satellite reflections remain absent if the pressure is released while the temperature is maintained at 20 K. It was proposed that the high pressure structural phase is ordered and the transition from the modulated

structure to the completely ordered phase accounts for the rise in T_c. The ordered structure was later confirmed with data obtained at the ILL.[35]

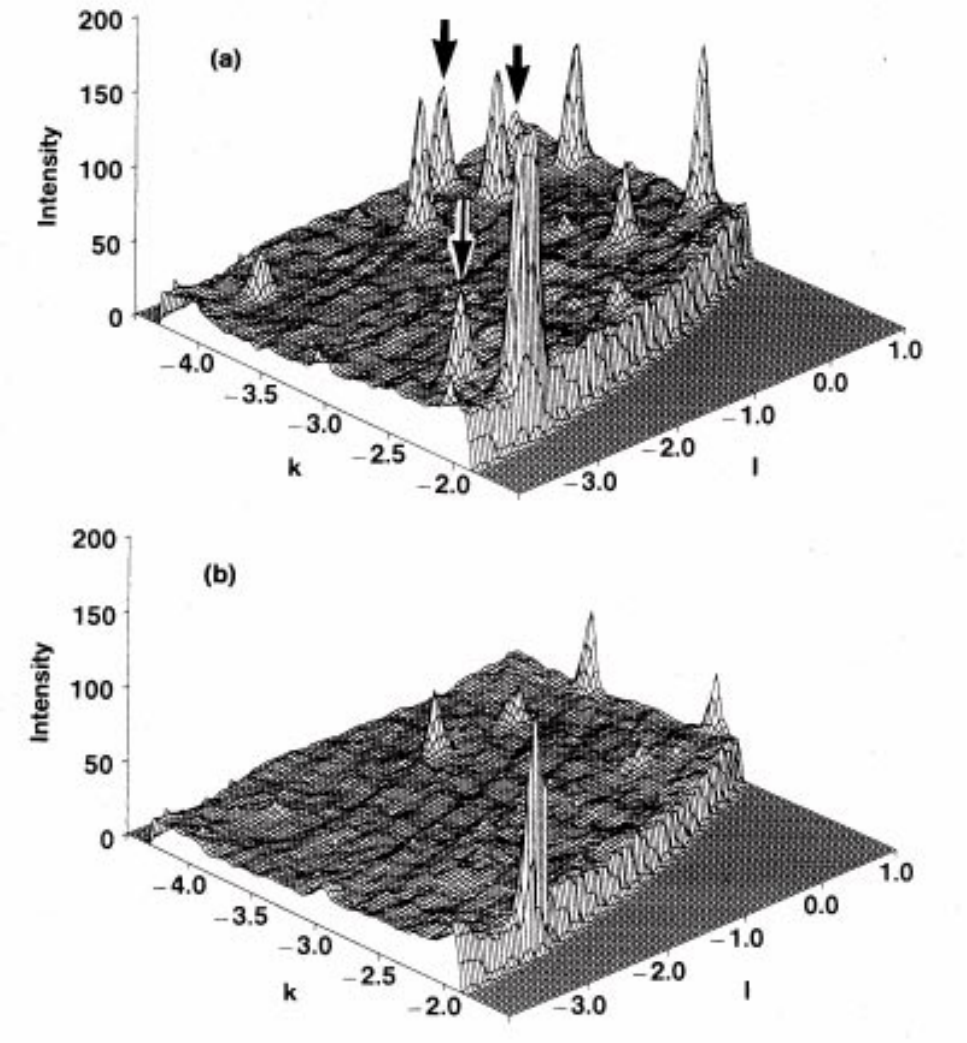

Figure 6. (a) Plot of the neutron-diffraction intensity distribution in the h = 4.92 reciprocal lattice plane of β-$(ET)_2I_3$ at 20 K and with zero pressure. Satellite peaks at $(5\ \bar{2}\ \bar{3})$–**q**, $(5\ \bar{4}\ 0)$–**q**, and $(5\ \bar{4}\ 1)$–**q** , where **q** = 0.08**a*** + 0.27**b*** + 0.21**c***, are clearly observable. (b) The same h = 4.92 plane after applying a pressure of 1.4 kbar, warming to room temperature, and cooling back down to 20 K.

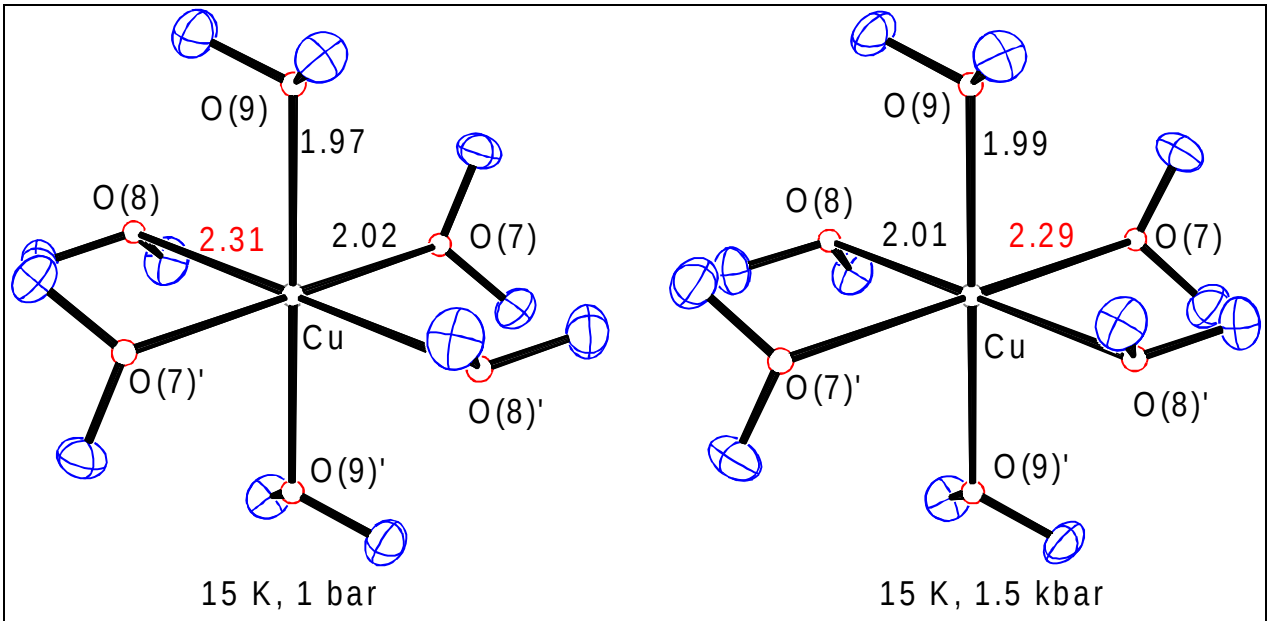

Figure 7. The coordination sphere around the copper atoms in $(ND_4)_2[Cu(D_2O)_6](SO_4)_2$ at (a) T = 15 K, P = 1 bar and (b) T = 15 K, P = 1.5 kbar. Note the switch in the Cu–O(7) and Cu–O(8) bond lengths between (a) and (b).

A Pressure-Switchable Jahn-Teller Distortion

Using the SCD helium pressure apparatus, the first example of a pressure-induced Jahn-Teller distortion switch was observed.[36] As shown in Figure 7, application of 1.5 kbar of pressure switches the long axis of the Jahn-Teller distortion by 90° in the deuterated ammonium copper Tutton's salt, $(ND_4)_2[Cu(D_2O)_6](SO_4)_2$. The Cu–O(7) bond length changes from 2.022(2) to 2.290(2) Å and the Cu–O(8) bond length changes from 2.310(2) to 2.014(2) Å. Thus, the high pressure phase of the deuterated salt is isostructural with the hydrogenous salt, but not with the alkali metal salts. The switching of the long axis of the Jahn-Teller distortion appears to be associated with a rotation of the ND_4^+ cation with concomitant changes in the hydrogen bonding of the coordinated water molecules with the SO_4^{2-} anions.

Structural and Magnetic Properties of La_2CuO_4-Type Materials

Oxygen deficient $La_2CuO_{4-\delta}$ is antiferromagnetic with a Néel temperature that depends on δ and a magnetic form factor in the ordered state which is not in very good agreement with that of

the Cu^{2+} free ion due to a plateau at low *Q*. The two reasons suggested for this discrepancy are either anisotropic magnetization density of the copper site or some small magnetic moment on the out-of-plane oxygen sites. In order to test these theories, measurements on a material in which the out-of-plane oxygen atoms are replaced by chlorine atoms, $Sr_2CuO_2Cl_2$, were carried out.[37] Using the SCD, it was found that the form factor of $Sr_2CuO_2Cl_2$ is quite similar to that of La_2CuO_4 and it is therefore unlikely that any significant moments exist on the out-of-plane oxygen (or Cl) ions. A reasonable fit to the experimental form factor data is obtained if a dipolar spin polarization on the in-plane oxygen ions is assumed. In this model, the in-plane oxygen 2p orbital which overlaps with the two nearest neighbor Cu d_{x2-y2} orbitals is spin-up on one side and spin down on the other side.

Since Ni^{2+} has a much larger moment than Cu^{2+}, measurements on La_2NiO_4 should be more precise than those on La_2CuO_4 and $Sr_2CuO_2Cl_2$. Attempts to measure the magnetic reflections of La_2NiO_4 at a steady state reactor source were not successful due to contamination by multiple Bragg scattering. Using the IPNS SCD, each reflection was measured many times (~10) over a wide range of neutron wavelengths so that anomalous intensities could be easily identified and discarded.[38] The experimentally determined data for La_2NiO_4 exhibit a plateau at low Q similar to La_2CuO_4 and $Sr_2CuO_2Cl_2$. With La_2NiO_4, the larger number of measured magnetic reflections permits the evaluation of the spin density Fourier map corresponding to the difference between the observed density and that obtained by fitting the data to an isotropic Ni^{2+}

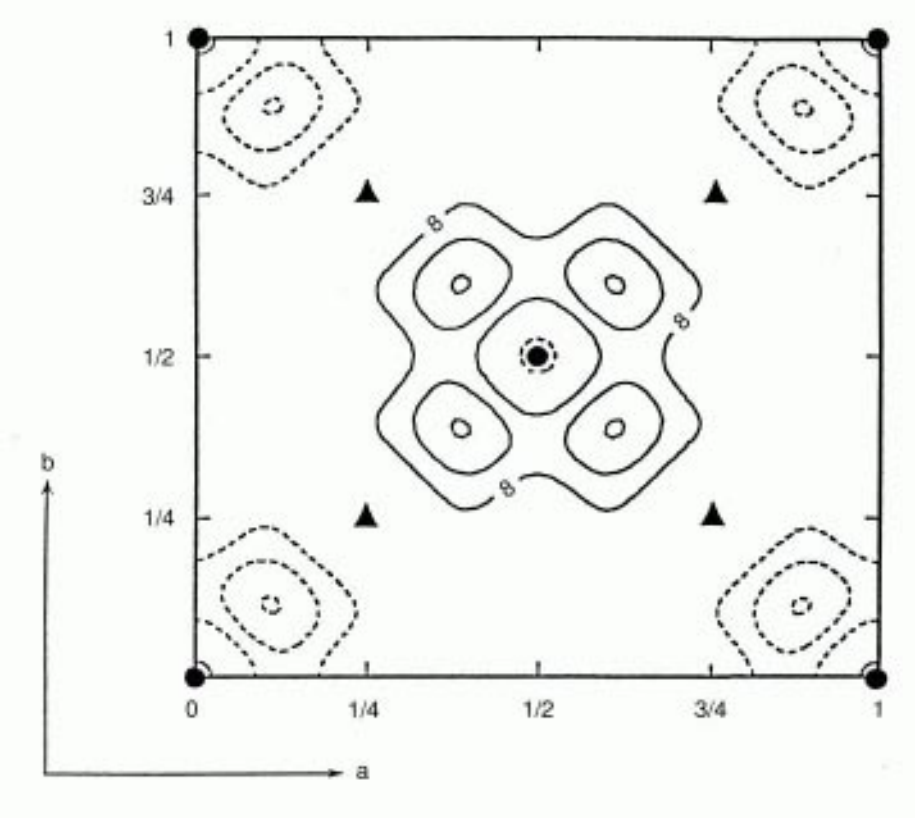

Figure 8. The difference magnetization density in the Ni-O plane of La_2NiO_4. The atoms symbols are circles for Ni and triangles for O. The solid and dashed contours denote positive and negative densities, respectively. Each contour is $8x10^{-3}$ $\mu_B/Å^3$. The Ni atoms at the corner positions have been defined to have positive densities.

form factor. No significant density is observed away from the Ni-O plane. As shown in Figure 8, in the Ni-O plane there is spin density extending from each copper in the direction of the four in-plane oxygen atoms.

Oxygen rich $La_2CuO_{4+\delta}$ is a superconductor with T_c = 40 K for δ = 0.1. A crystal prepared by room temperature electrochemical oxidation of La_2CuO_4 was studied on the SCD[19] and appears to be single phase with *Fmmm* symmetry and with the excess oxygen located between adjacent LaO layers from analysis of the fundamental Bragg peaks. In addition, satellites arising from a modulation could be clearly identified in the single-crystal data, as shown in Figure 9. The

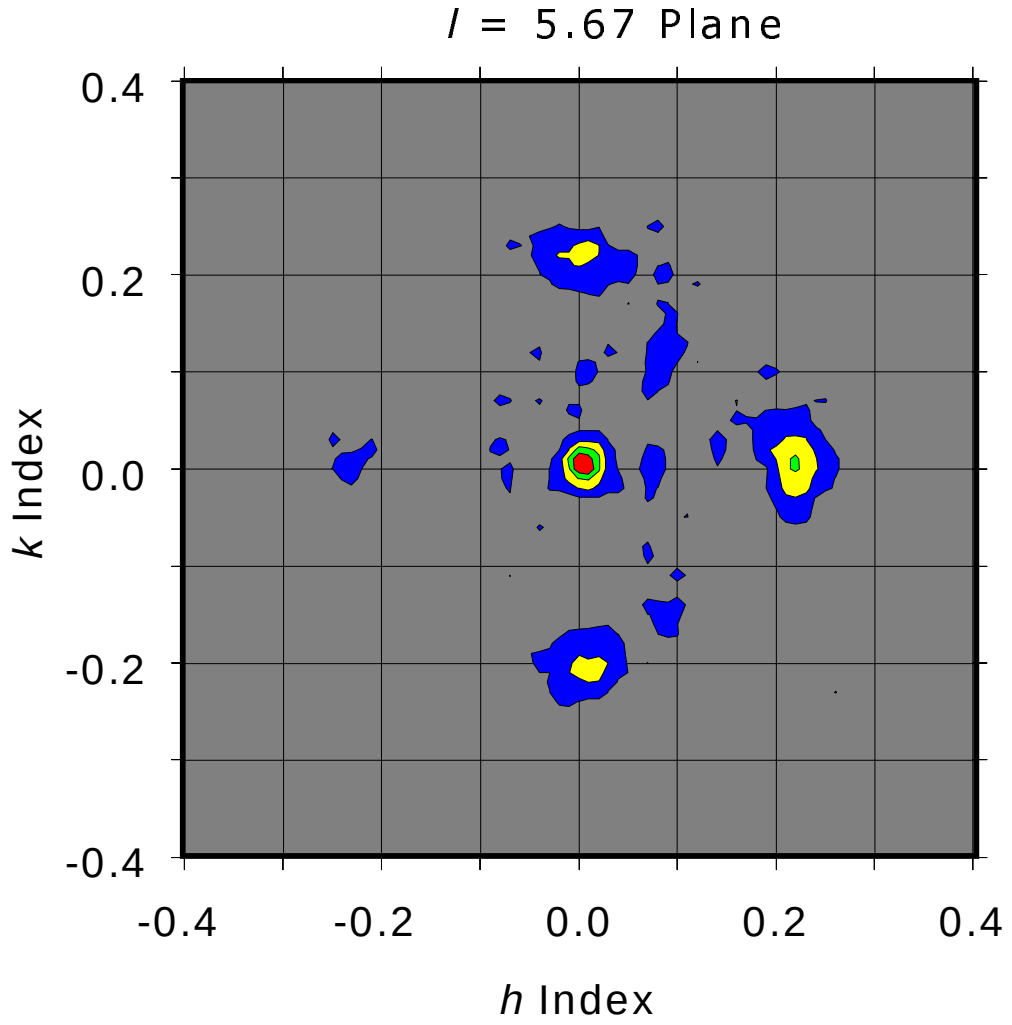

Figure 9. Intensity contour plot of reciprocal space perpendicular to the c^* direction at l = 5.67 from a single crystal of oxygen rich $La_2CuO_{4+\delta}$. Satellites with proppatation vectors (0, ±0.2, -0.333) appear around the tail of the [0,0,6] Bragg reflection.

reciprocal lattice defined by the satellites appears to be commensurate with the original one: all observed reflections can be indexed using an *F* centered $10a \times 10b \times 6c$ supercell. However, due to twinning, the observed satellite pattern could result from the superposition of more than one set of superlattice reflections, each with a smaller supercell. An experiment on a detwinned crystal is planned for the future.

SUMMARY

With the start-up of several pulsed spallation neutron sources in the 1980's, the single-crystal TOF Laue technique has been successfully exploited for a broad range of scientific applications, including chemical crystallography, phase transitions, magnetic scattering, and diffuse scattering. In particular, the ability to easily survey large volumes of reciprocal space, to obtain data at high ***Q*** vectors, to design and use environmental equipment with minimal alignment and motion requirements, are some of the advantages of this technique. Progress in the development of the technique and the instrumentation will continue and should lead to greater advances with the increasing fluxes available from existing sources and with the potential for much higher fluxes from proposed new sources.

ACKNOWLEDGEMENT

Work at Argonne National Laboratory was sponsored by the U.S. Department of Energy, Office of Basic Energy Sciences, Division of Materials Sciences, under Contract W-31-109-ENG-38.

REFERENCES

1. R. D. Lowde, *Acta Cryst.* **9**, 151 (1956).
2. A. J. Schultz, *Trans. Am. Crystallogr. Assoc.* **23**, 61 (1987).
3. R. W. Alkire, A. C. Larson, P. J. Vergamini and B. Morosin, *Acta Cryst. C* **41**, 1709 (1985).

4. J. B. Forsyth, R. T. Lawrence and C. C. Wilson, *Nucl. Instr. Meth. Phys. Res. A* **273**, 741 (1988).
5. N. Niimura, K. Yamada, T. Kubota, A. Matsumoto and S. Hoshino, *Nucl. Instrum. Methods* **211**, 203 (1983).
6. H.-R. Wenk, *Trans. Am. Crystallogr.* **29**, companion paper in this volume (1993).
7. D. A. Keen, *Trans. Am. Crystallogr. Assoc.* **29**, companion paper in this volume (1993).
8. B. Buras, K. Mikke, B. Lebech and J. Leciejewicz, *Phys. Stat. Sol.* **11**, 567 (1965).
9. D. H. Day and R. N. Sinclair, *Acta Cryst. B* **26**, 2079 (1970).
10. A. M. Balagurov, E. Borca, M. Dlouha, Z. Ghkeorghiu, G. M. Mironova and V. B. Zlokazov, *Acta Cryst. A* **35**, 131 (1979).
11. N. Niimura, T. Kubota, M. Sato, M. Arai and Y. Ishikawa, *Nucl. Instrum. Methods* **173**, 517 (1980).
12. S. W. Peterson, A. H. Reis Jr., A. J. Schultz and P. Day, in *Solid State Chemistry: A Contemporary Overview*, S. L. Holt, J. B. Milstein, M. Robbins, Ed. (American Chemical Society, Washington, D. C., 1980), pp. 75.
13. A. J. Schultz, R. G. Teller, S. W. Peterson and J. M. Williams, in *Neutron Scattering—1981*, J. Faber Jr., Ed. (American Institute of Physics, New York, 1982), pp. 35.
14. W. Jauch, G. J. McIntyre and A. J. Schultz, *Acta Cryst. B* **46**, 739 (1990).
15. W. Jauch, A. Palmer and A. J. Schultz, *Acta Cryst. B* in press (1993).
16. W. Jauch, *Trans. Am. Crystallogr. Assoc.* **29**, companion paper in this volume (1993).
17. R. J. Nelmes, C. J. Howard, T. W. Ryan, W. I. F. David, A. J. Schultz and P. C. W. Leung, *J. Phys. C: Solid State Phys.* **17**, L861 (1984).
18. T. J. Emge, P. C. W. Leung, M. A. Beno, A. J. Schultz, H. H. Wang, L. M. Sowa and J. M. Williams, *Phys. Rev. B* **30**, 6780 (1984).
19. P. G. Radaelli, J. D. Jorgensen, A. J. Schultz, B. A. Hunter, J. L. Wagner, F. C. Chou and D. C. Johnston, *Phys. Rev. B* **48**, 449 (1993).

20. H.-R. Wenk, A. C. Larson, P. J. Vergamini and A. J. Schultz, *J. Appl. Phys.* **70**, 2035 (1991).
21. A. J. Schultz, R. G. Teller, J. M. Williams, M. G. Strauss and R. Brenner, *Trans. Am. Crystallogr. Assoc.* **18**, 169 (1982).
22. R. A. Jacobson, *J. Appl. Cryst.* **19**, 283 (1986).
23. C. Wilkinson and A. J. Schultz, *J. Appl. Cryst.* **22**, 110 (1989).
24. C. Wilkinson, H. W. Khamis and R. F. D. Stansfield, *J. Appl. Cryst.* **21**, 471 (1988).
25. A. J. Schultz and P. C. W. Leung, *J. de Physique Colloque C5* **47**, 137 (1986).
26. H. Horiuchi, A. J. Schultz, P. C. W. Leung and J. M. Williams, *Acta Cryst. B* **40**, 367 (1984).
27. W. T. A. Harrison, T. E. Gier, G. D. Stucky and A. J. Schultz, *J. Chem. Soc., Chem. Commun.* 540 (1990).
28. A. J. Schultz, R. G. Teller, M. A. Beno, J. M. Williams, M. Brookhart, W. Lamanna and M. B. Humphrey, *Science* **220**, 197 (1983).
29. P. C. W. Leung, A. J. Schultz, H. H. Wang, T. J. Emge, G. A. Ball, D. D. Cox and J. M. Williams, *Phys. Rev. B* **30**, 1615 (1984).
30. J. M. Williams, A. J. Schultz, U. Geiser, K. D. Carlson, A. M. Kini, H. H. Wang, W.-K. Kwok, M.-H. Whangbo and J. E. Schirber, *Science* **252**, 1501 (1991).
31. P. C. W. Leung, T. J. Emge, M. A. Beno, H. H. Wang, J. M. Williams, V. Petricek and P. Coppens, *J. Am. Chem. Soc.* **107**, 6184 (1985).
32. V. N. Laukhin, E. É. Kostyuchenko, Y. V. Sushko, I. F. Shchegolev and É. B. Yagubskii, *JETP Lett.* **41**, 68 (1985).
33. K. Murata, M. Tokumoto, H. Anzai, H. Bando, G. Saito, K. Kajimura and T. Ishiguro, *J. Phys. Soc. Jpn.* **54**, 1236 (1985).
34. A. J. Schultz, M. A. Beno, H. H. Wang and J. M. Williams, *Phys. Rev. B* **33**, 7823 (1986).
35. A. J. Schultz, H. H. Wang, J. M. Williams and A. Filhol, *J. Am. Chem. Soc.* **108**, 7853 (1986).

36. C. J. Simmons, M. A. Hitchman, H. Stratemeier and A. J. Schultz, *J. Am. Chem. Soc*. in press (1993).
37. X. L. Wang, L. L. Miller, J. Ye, C. Stassis, B. N. Harmon, D. C. Johnston, A. J. Schultz and C.-K. Loong, *J. Appl. Phys.* **67**, 4524 (1990).
38. X.-L. Wang *et al.*, *Phys. Rev. B* **45**, 5645 (1992).